CCIT Report #621

May 2007

LOCAL VERSUS GLOBAL IN QUASI-CONFORMAL MAPPING FOR MEDICAL IMAGING

EMIL SAUCAN, ELI APPLEBOIM, EFRAT BARAK, RONEN LEV AND YEHOSHUA Y. ZEEVI

Abstract. A method and algorithm of flattening of folded surfaces for two-dimensional representation and analysis of medical images are presented. The method is based on extension of classical results of Gehring and Väisälä regarding the existence of quasi-conformal and quasi-isometric mappings.

The proposed algorithm is basically local and, therefore, suitable for extensively folded surfaces encountered in medical imaging. The theory and algorithm guarantee minimal distance, angle and area distortion. Yet, it is relatively simple, robust and computationally efficient, since it does not require computational derivatives. Both random starting point and curvature-based versions of the algorithm are presented.

We demonstrate the algorithm using medical data obtained from real CT images of the colon and MRI scan of the human cortex.

Further applications of the algorithm, for image processing in general are also considered.

Moreover, the globality of this algorithm is also studied, via extreme length methods for which we develop a technique for computing straightest geodesics on polyhedral surfaces.

1. Introduction

2D representation by flattening of 3D object scans is a fundamental step, required in medical volumetric imaging. For example, it is often required to present three-dimensional fMRI scans of the brain cortex as flat two-dimensional images. In the latter case it is possible, for example, to better observe and follow up developments of neural activity within the folds. Flattening of 3D-scans is in particular important in CT virtual colonoscopy; a non-invasive, rapidly advancing, imaging procedure capable of determining the presence of colon pathologies such as small polyps [16]. However, because of the extensive folding of the colon, rendering of the 3D data for detection of pathologies requires the implementation of cylindrical or planar map projections [17]. In order to map such data in a meaningful manner, so that diagnosis will be accurate, it is essential that the geometric distortion, in terms of angles and lengths, caused by the representation, will be minimal. Due to these medical applications, this problem has attracted a great deal of attention in the last few years.

Date: March 20, 2007.

1.1. **Related Works.** As stated above, the problem of minimal distortion flattening of surfaces attracted, in recent years, a great attention and interest, due to its wide range of applications.

In this section we briefly review some of the methods that were proposed for dealing with this problem.

1.1.1. *Variational Methods.* Haker et al. ([16], [17]) introduced the use of a variational method for conformal flattening of CT/MRI 3-D scans of the brain/colon for the purpose of medical imaging. The method is essentially based on solving Dirichlet problem for the Laplace-Beltrami operator $\triangle u = 0$ on a given surface Σ, with boundary conditions on $\partial\Sigma$. A solution to this problem is a harmonic (thus conformal) map from the surface to the (complex) plane. The solution suggested in [16] and [17] is a PL (piecewise linear) approximation of the smooth solution, achieved by solving a proper system of linear equations. A further development of this method, based upon the existence of a area-minimizing diffeomorphism between surfaces is given in [2].

1.1.2. *Circle Packing.* Hurdal et al. ([21]) attempt to obtain such a conformal map by using circle packing. This relies on the ability to approximate conformal structure on surfaces by circle packings. The authors use this method for MRI brain images and conformally map them to the three possible models of geometry in dimension 2 (i.e. the 2-sphere, the Euclidian plane and the Hyperbolic plane). Yet, the method is applicable for surfaces which are topologically equivalent to a disk whereas the brain cortex surface is not. This means that there is a point of the brain (actually a neighborhood of a point), which will not map conformally to the plane, and in this neighborhood the dilatation will be infinitely large. An additional problem arises due to the necessary assumption that the surface triangulation is homogeneous in the sense that all triangles are equilateral. Such triangulations are seldom attainable.

1.1.3. *Conformal Modulus.* In the sequel [22] of their previously cited work, Hurdal and Stephenson employ *conformal modulus*, computed by *extremal length* methods, mainly to extract(compute) local features in the mapping of the human cerebellum.

1.1.4. *Holomorphic 1-forms.* Gu et al. ([14], [15], [13]) are using holomorphic 1-forms in order to compute global conformal structure of a smooth surface of arbitrary genus given as a triangulated mesh. holomorphic 1-forms are differential forms (differential operators) on smooth manifolds, which among other things can depict conformal structures. The actual computation is done via computing homology/co-homology bases for the first homology/co-homology groups of the surface, H_1, H^1 respectively. This method indeed yields a global conformal structure hence, a conformal parameterization for the surface however, computing homology basis is extremely time consuming.

1.1.5. *Angle Methods.* In [31] Sheffer et al. parameterize surfaces via an angle based method in a way that minimizes angle distortion while flattening. However, the surfaces are assumed to be approximated by cone surfaces, i.e. surfaces that are composed from cone-like neighborhoods.

In all the above-mentioned methods the outcome is in fact not a conformal map but a quasi-conformal map. This fact implies that all the geometric measures are kept up to some bounded distortion. Yet, sometimes the resultant distortion may render the data to become unacceptable. This is due to the fact that, in general, a surface is only locally conformal to the plane so, if one tries to flatten a surface in some manner of globality, the best result is obtained by means of a quasi-conformal flattening. Given this fact, it would be desirable to have a precise bound on the distortion caused by the flattening. However, none of the mentioned methods is capable of yielding such a bound.

The main algorithm presented in this paper proposes yet another solution to this problem. The proposed method relies on theoretical results obtained by Gehring and Väisälä in the 1960's ([12]). They were studying the existence of quasi-conformal maps between Riemannian manifolds. The basic advantages of this method resides in its simplicity, in setting, implementation and its speed. Additional advantage is that it is possible guarantee not to have distortion above a predetermined bound, which can be as small as desired, with respect to the amount of localization one is willing to pay (and, in the case of triangulated surfaces, to the quality of the given mesh). In fact, the proposed method is – to the best of our knowledge – the only algorithm capable of computing both length distortion and angle dilatation. The suggested algorithm is best suited to cases where the surface is complex (high and non-constant curvature) such as brain cortex/colon wrapping, or of large genus, such as skeleta, proteins, etc. Moreover, since together with the angular dilatation, both length and area distortions are readily computable, the algorithm is ideally suited for applications in Oncology, where such measurements are highly relevant.

The proposed method is basically local. In order to assess the extent at which this method can be made global we use the conformal modulus as measure. We test this approach on CT-scans of the human colon. This requires the computation of geodesics on the colon surface which is a topological cylinder. In this paper we propose a modified version of an algorithm due to Polthier and Schmies [27] for finding *straightest geodesics* on triangulated surfaces.

In addition, we consider the use of the presented algorithm in the wider context of image processing.

The body of the paper is organized as follows: In Section 2 we bring the necessary background material: quasi-conformal and quasi-isometric mappings, admissible surfaces, moduli of quadrilaterals and rings and the extremal length method; as well as some basic facts on quasi-geodesics on polyhedral surfaces. Section 3 is dedicated to the presentation of our main algorithms: the global one, based on conformal moduli, and where we apply a surface dissection method using PL-quasi-geodesics; and the local one stemming from the seminal work of Gehring and Väisälä/ The following section is dedicated to the analysis of the experimental results, for both our main algorithms. In addition, an application of admissible surfaces to the analysis of black-and-white images is also included here. Finally, in Section 5 we sum-up the methods and results presented and consider a number of further developments and improvements.

2. Theoretical Background

2.1. Quasi-Conformal Mappings.

Definition 2.1. Let $D \subseteq \mathbb{R}^n$ be a domain; $n \geq 2$ and let $f : D \to \mathbb{R}^n$ be a homeomorphism. f is called *quasi-conformal* iff
(i) f belongs to $W^{1,n}_{loc}(D)$,
and
(ii) there exists $K \geq 1$ such that:

$$|f'(x)|^n \leq K J_f(x)\ a.e.\,; \tag{2.1}$$

where $f'(x)$ denotes the formal derivative of f at x, $|f'(x)| = \sup_{|h|=1} |f'(x)h|$, and where $J_f(x) = det f'(x)$. The smallest number K that satisfies (2.1) is called the *outer dilatation*, $K_O(f)$, of f.

One can extend the above definitions to oriented, connected $\mathcal{C}^\infty$ Riemannian manifolds as follows:

Definition 2.2. Let M^n, N^n be oriented, connected $\mathcal{C}^\infty$ Riemannian n-manifolds, $n \geq 2$, and let $f : M^n \to N^n$ be a continuous function. f is called *locally quasi-conformal* iff for every $x \in M^n$, there exist coordinate charts (U_x, φ_x) and $(V_{f(x)}, \psi_{f(x)})$, such that $f(U_x) \subseteq V_{f(x)}$ and $g = \psi_{f(x)} \circ f \circ \varphi_x^{-1}$ is quasi-conformal.

If f is locally quasi-conformal, then $T_x f : T_x(M^n) \to T_{f(x)} N^n$ exists for a.e. $x \in M^n$.

Definition 2.3. Let M^n, N^n be oriented, connected $\mathcal{C}^\infty$ Riemannian n-manifolds, $n \geq 2$, and let $f : M^n \to N^n$ be a homeomorphism. f is called *quasi-conformal* iff

(1) f is locally quasi-conformal and
(2) there exists $K, 1 \leq K < \infty$, such that

$$|T_x f|^n \leq K J_f(x) \tag{2.2}$$

for a.e. $x \in M^n$.

If f is quasi-conformal, then there exists $K \geq 1$ such that the following inequality holds a.e. in M^n:

$$J_f(x) \leq K' \cdot \inf_{|h|=1} |T_x f h|^n \tag{2.3}$$

By analogy with the outer dilatation we have the following definition:

Definition 2.4. The smallest number K' that satisfies inequality (2.3) is called the *inner dilation* $K_I(f)$ of f. The *maximal dilatation* of f is defined as $\max(K_O(f), K_I(f))$. A mapping f is called K-*quasi-conformal* iff there exists $K \geq 1$ such that $K(f) \leq K$.

The dilatations are simultaneously finite or infinite. Indeed, the following inequalities hold:

$$K_I(f) \leq K_O^{n-1}(f) \text{ and } K_O(f) \leq K_I^{n-1}(f)\,.$$

In some cases(applications) it is more convenient to employ(make appeal to) the *metric definition of quasi-conformality*, via(by means of) the *linear dilatation*:

$$H(x,f) = H\big(f'(x)\big) = \frac{\max_{|h|\,=\,1} |f'(x)h|}{\min_{|h|\,=\,1} |f'(x)h|}\,.$$

The following relationship between the maximal and linear dilatations holds:

$$H(x,f) \leq K^{2/n}, \text{ for all } x \in D.$$

2.1.1. *Quasi-Isometries and Projections.*

Definition 2.5. Let $D \subset \mathbb{R}^n$ be a domain. A homeomorphism $f : D \to \mathbb{R}^n$ is called a *quasi-isometry* (or a *bi-lipschitz mapping*), if there exists $1 \leq C < \infty$ such that

$$\frac{1}{C}|p_1 - p_2| \leq |f(p_1) - f(p_2)| \leq C|p_1 - p_2|\,, \text{ for all } p_1, p_2 \in D; \tag{2.4}$$

where "$|\cdot|$" denotes the standard (Euclidean) metric on $\mathbb{R}^n$.

$C(f) = \min\{C \,|\, f \text{ is a quasi} - \text{isometry}\}$ is called the *minimal distortion* of f (in D).

Remark 2.6. Evidently, the above definition readily extends to general metric spaces. In particular, for the case of hypersurface embedded in $\mathbb{R}^n$, distances are the induced intrinsic distances on the surface.

Definition 2.7. Let D be a domain in $\mathbb{R}^n$ and let $f : D \to \mathbb{R}^n$ be a mapping. f is called a *local* C-*quasi-isometry* (in D) iff for every $C' > C$ and for any $x \in D$, there exist a neighbourhood $U_x \subset D$ of x, such that $f|_{U_x}$ is a quasi-isometry with maximal dilatation C'.

Local quasi-isometries have an important physical interpretation: Let $C(D) = \sup\{C \,|\, \text{any f local C}-\text{quasi} - \text{isometry is injective in D}\}$. Then, if D is regarded as an elastic body and f as deformation of D under the influence of a force field, then $C(D)$ represents the critical strain, i.e. the strain under which D collapses onto itself.

If f is a quasi-isometry, then

$$K(f) \leq C(f)^{2(n-1)}. \tag{2.5}$$

It follows that any quasi-isometry is a quasi-conformal mapping (while, evidently, not every quasi-conformal mapping is a quasi-isometry).

Definition 2.8. Let $S \subset \mathbb{R}^n$ be a connected, $(n-1)$-dimensional set. S is called *admissible* (or an *admissible hypersurface*) iff for any $p \in S$, there exists a quasi-isometry i_p such that for any $\varepsilon > 0$ there exists a neighbourhood $U_p \subset \mathbb{R}^n$ of p, such that $i_p : U_p \to \mathbb{R}^n$ and $i_p(S \cap U_p) = D_p \subset \mathbb{R}^{n-1}$, where D_p is a domain, and such that $C(i_p)$ satisfies:

$$(i)\ \sup_{p \in S} C(i_p) < \infty\,;$$

and

$$(ii)\ \operatorname{ess\,sup}_{p \in S} C(i_p) \leq 1 + \varepsilon\,.$$

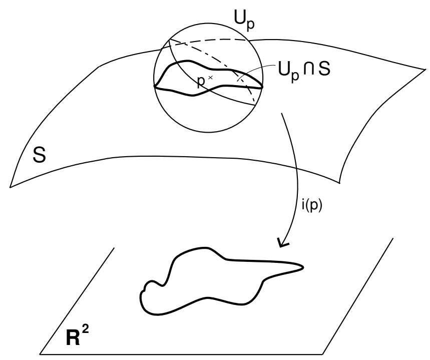

Figure 1. An Admissible Surface

Let $S \subset \mathbb{R}^n$ be a set homeomorphic to an $(n-1)$-dimensional domain, $\vec{n}$ be a fixed unitary vector, and $p \in S$, such that there exists a neighbourhood $V \subset S$, such that $V \simeq D^{n-1}$, where $D^{n-1} = \{x \in \mathbb{R}^{n-1} \,\big|\, ||x|| \leq 1\}$. Moreover, suppose that for any $q_1, q_2 \in S$, the acute angle $\measuredangle(q_1q_2, \vec{n}) \geq \alpha$. We refer to the last condition as *the Geometric Condition* or *Gehring Condition* (see [12]).

Then, for any $x \in V$ there exists a unique representation of the following form:

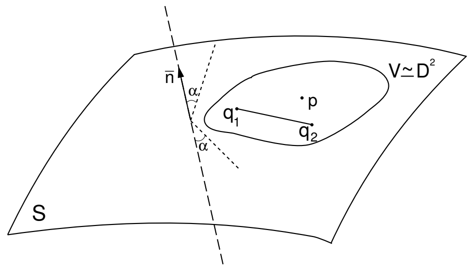

FIGURE 2. The Geometric Condition

$$x = q_x + u\vec{n}\,;$$

where q_x lies on the hyperplane through p, which is orthogonal to $\vec{n}$ and $u \in \mathbb{R}$.

Define:

$$Pr(x) = q_x\,.$$

Remark 2.9. $\vec{n}$ need not be the normal vector to S at p.

By [9], Corollary 1, p. 338, we have that for any $p_1, p_2 \in S$ and any $a \in \mathbb{R}_+$ the following inequalities hold:

$$\frac{a}{A}\,|p_1 - p_2| \leq |Pr(p_1) - Pr(p_2)| \leq A|p_1 - p_2|\,;$$

where

$$A = \frac{1}{2}[(a\csc\alpha)^2 + 2a + 1]^2 + \frac{1}{2}[(a\csc\alpha)^2 - 2a + 1]^2\,.$$

In particular, for $a = 1$ we get that

$$C(f) \leq \cot\alpha + 1 \tag{2.6}$$

and

$$K(f) \leq \Big((\frac{1}{2}(\cot\alpha)^2 + 4)^{\frac{1}{2}} + \frac{1}{2}\cot\alpha\Big)^n \leq (\cot\alpha + 1)^n\,. \tag{2.7}$$

From the above discussion we conclude that $S \subset \mathbb{R}^3$ is an admissible hypersurface if for any $p \in S$ there exists $\vec{n}_p$ such that for any $\varepsilon > 0$ there exists $U_p \simeq D^2$ such that for any $q_1, q_2 \in U_p$ the acute angle $\measuredangle(q_1q_2, \vec{n}_p) \geq \alpha$, where

$$(i)\ \inf_{p\in S} \alpha_p > 0\,;$$

and

$$(ii)\ \operatorname{ess}\inf_{p\in S}\alpha_p \geq \frac{\pi}{2} - \varepsilon\,.$$

Example 2.10. Any hypersurface in $S \in \mathbb{R}^3$, that admits a well-defined continuous turning tangent plane at any point $p \in S$ is admissible.

Definition 2.11. Let S_1, S_2 be two admissible surfaces and let $f : S_1 \to S_2$ be a homeomorphism (between them). Let $p_1 \in S_1$ be a generic point of S_1 and denote $p_2 = f(p_1)$. Let $i_{p_1} : U_{p_1} \to D_{p_1}, i_{p_2} : U_{p_2} \to D_{p_2}$ denote the quasi-isometries associated with p_1, p_2, respectively. f is called K-*quasi-conformal* iff $K(g_p)$ satisfies the following inequalities:

$$(i)\ \sup_{p\in S} K(g_p) < \infty\,,$$

and

$$(ii)\ \operatorname{ess}\sup_{p\in S} K(i_p) \leq K + \varepsilon\,;$$

where K_{g_p} denotes the maximum dilatation of $g_{p_1} = i_{p_1} \circ f \circ i_{p_2}^{-1}$. The smallest number K for which f is K-quasi-conformal is called the maximal dilatation of f and is denoted by $K(f)$.

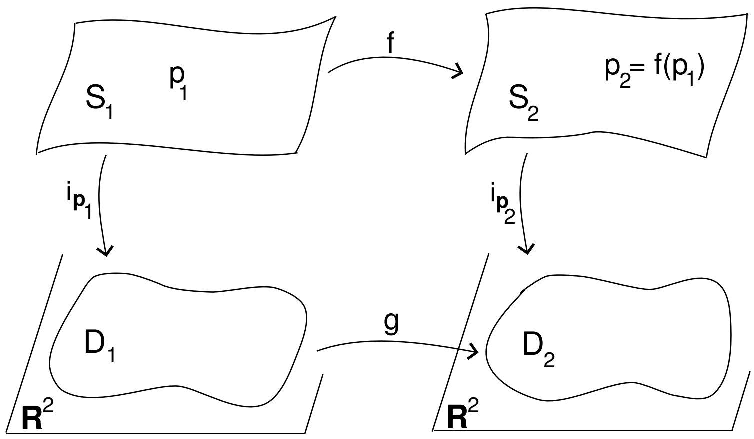

FIGURE 3

Furthermore, the dilatations of f and g_{p_1} and the distortions of i_{p_1} and i_{p_2} are interrelated by the following inequality:

$$K_{g_p} \leq K C(i_{p_1})^{2(n-1)} C(i_{p_1})^{2(n-1)}. \tag{2.8}$$

2.2. **Conformal Modulus and Extremal Length.**

2.2.1. *The Conformal Modulus.*

Definition 2.12. A *quadrilateral* is a simply connected planar domain Q together with four points $z_1, z_2, z_3, z_4 \in \partial Q$, where the order of the points z_1, z_2, z_3, z_4 agrees with the positive orientation on ∂Q. The points z_1, z_2, z_3, z_4 are called the *vertices* of Q and the arcs determined by z_1, z_2, z_3, z_4 on ∂Q are called the *sides* of Q: $\widehat{z_1z_2}, \widehat{z_3z_4}$ are called the a-*sides* and $\widehat{z_2z_3}, \widehat{z_4z_1}$ are called the b-*sides*.

From the Riemann Mapping Theorem (see, e.g. [25], p. 13) it follows that any any quadrilateral may be mapped on the quadrilateral $Q'(-\frac{1}{k}, -1, 1, \frac{1}{k})$, $0 < k < 1$; where Q' is the upper half-plane.

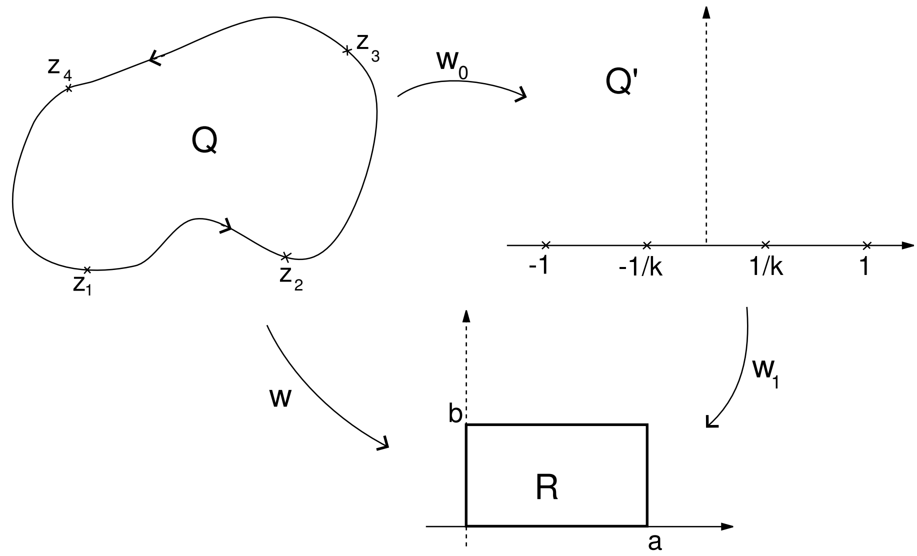

FIGURE 4

Since any three points on the boundary of Q determine the mapping completely, it follows that quadrilaterals are partitioned into equivalence classes.

By classical results in elliptic function theory it follows that

$$w_1(z) = \int_0^z \frac{d\zeta}{\sqrt{(1-\zeta^2)(1-k^2\zeta^2)}}$$

maps $Q'(-\frac{1}{k}, -1, 1, \frac{1}{k})$ onto a rectangle R. If w_0 denotes the mapping from Q onto Q', then the *canonical mapping of* Q: $w = w_1 \circ w_0$ maps the quadrilateral Q conformally onto the *canonical rectangle* $R = R(Q) = \{x+iy \,|\, 0 < x < a, 0 < y < b\}$. Therefore, any conformal class of equivalence of quadrilaterals contains rectangles. Conversely, any conformal mapping between two rectangles is a similarity transformation. Moreover, since similar rectangles obviously belong to the same equivalence class, all canonical rectangles of a given quadrilateral Q have the same ratio of the sides $a/b = M(Q)$ (hence the denomination of the a-sides and b-sides). The number $M(Q)$ is called the *conformal module* (*modulus*) of the quadrilateral Q. It follows from the discussion above that two quadrilaterals are conformally equivalent iff they have the same module.

Remark 2.13. $M\big(Q(z_1,z_2,z_3,z_4)\big) = M\big(Q(z_3,z_4,z_1,z_2)\big) = 1/M\big(Q(z_2,z_3,z_4,z_1)\big)$.

2.2.2. *Extremal Length – The Length-Area Method.* The extremal length method – introduced by Beurling in 1946 – represents the sought for tool for computing the moduli of quadrilaterals:

$$M(Q) = \frac{\int\int |w'(z)|^2 d\sigma}{\big(\inf_{\beta\in\mathcal{C}_a}\int_C |w'(z)||dz|\big)^2}\,. \tag{2.9}$$

Here $\mathcal{C}_a$ denotes the family of locally rectifiable Jordan arcs included in Q, that connect the a-sides of Q and w denotes the canonical mapping of Q onto the canonical rectangle R.

The problem with the estimate above resides in the fact that it is given by using a certain conformal (i.e. 1-quasi-conformal mapping). Therefore a definition of the modulus of a quadrilateral that makes no appeal to quasi-conformality is desirable. Fortunately enough, such a definition exists and is given by the following formula:

$$M(Q) = \inf_{\varrho\in\mathcal{P}} \frac{m_\varrho(Q)}{\big(\inf_{\beta\in\mathcal{C}_a} l_\varrho(\beta)\big)^2}\,. \tag{2.10}$$

Here $\mathcal{P}$ denotes the family of non-negative Borel-measurable functions on Q, such that $\int_\beta \varrho(z)|dz| \geq 1$, for all $\beta \in \mathcal{C}_a$. The infimum is attained for $\varrho = |w'|$, where w is the canonical mapping of Q.

2.2.3. *The Modulus of a Ring.* One can also define the modulus of a *ring domain* R, i.e. of a doubly connected planar domain. This is done in analogy to the definition of the modulus of a quadrilateral, but in this case one maps conformally R onto an *annulus* $A = \{0 \leq r_1|z| \leq r_2 \leq \infty\}$. Here we will consider only *proper* annuli, i.e. such that $r_1 \neq 0, r_2 \neq \infty$. In this non-degenerate case, the modulus of the ring R is defined as $M(R) = \log\frac{r_2}{r_1}$.

As expected, there is a close connection between the moduli of the two types of domains. Indeed, given an annulus A of radii r_1, r_2, one can cut it along the segment $[r_1, r_2]$, and conformally map it onto a quadrangle Q. The foreseen result holds, i.e. the moduli of R and Q are equal.

The extremal methods applied in the case of quadrangles are also valid for rings and rend formulas similar to (2.9) and (2.10), which, for the test function $\varrho \equiv 1$ become:

$$M(R) = 2\pi \frac{min_c(length(c))^2}{Area(R)}\,; \tag{2.11}$$

and

$$M(R) = 2\pi \frac{Area(R)}{min_\gamma(length(\gamma))^2}\,; \tag{2.12}$$

respectively, where α and γ are types of curves depicted in the figure below, i.e. γ is a locally rectifiable arc connecting the two boundary components of R, $\partial_1 R$ and $\partial_2 R$, and α is a locally rectifiable simple closed curve, separating $\partial_1 R$ and $\partial_2 R$.

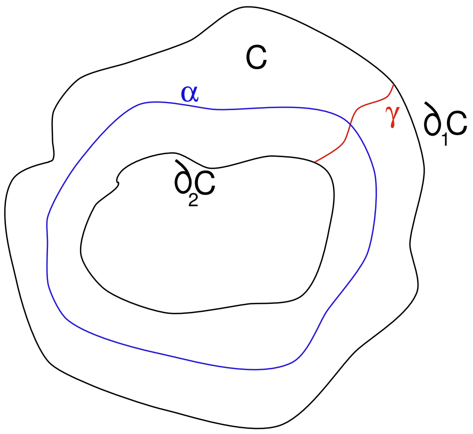

FIGURE 5

2.2.4. *Quasi-Conformal Mappings Between Annuli.* Let R, R' be annuli, and $f : R \to R'$ be a K-quasi-conformal mapping of R onto R'. Then:

$$\frac{1}{K} \leq \frac{M(R')}{M(R)} \leq K\,. \tag{2.13}$$

Note that, again, a parallel result holds for quadrangles.

2.3. **Quasi-geodesics on Polyhedral Surfaces.** In any path-metric spaces the natural definition of geodesics is that of shortest curves. Therefore in any combinatorial (including PL) context, the notion of "shortest path" designates *global shortest* path, with the obvious implementation short-comings. Thus, one is faced with a properly classical combinatorial (and computationally hard) problem of finding paths with global shortest length.

However, in differential geometry geodesics are classically defined *locally* as *straightest* paths. This is a straightforward generalization stemming from one of the characterizations of Euclidean lines (see [19]). For smooth (differentiable) surfaces (and higher dimensional manifolds) the condition a curve must satisfy to be a geodesic is that: $k_g \equiv 0$, where k_g denotes the *geodesic curvature* (see [10]). It is a classical result of differential geometry that geodesics are precisely the *locally shortest paths* (see, e.g. [10], Propositions 4.6.4 and 4.6.5). Note that k_g is an intrinsic notion, i.e it depends solely upon the inner geometry (metric) of the surface (manifold), and not upon its embedding in $\mathbb{R}^2$ ($\mathbb{R}^n$) (see, e.g. [7], Lemma 1.6.3). Also, it is important to recall that uniqueness and shortness of geodesic hold only locally, as the well known examples of the sphere and (right circular) cylinder illustrate. Moreover, even the global existence of shortest geodesics is not assured for all surfaces (manifolds), as the example of $\mathbb{R}^2 \setminus \{0\}$ with the Euclidean metric shows.

The following widely cited differential geometric criterion for a curve (e.g. on a surface) to be a geodesic:

$$\frac{d^2u^i}{ds^2} + \sum_{j,k=1}^{2} \Gamma^i_{jk} \frac{du^j}{ds}\frac{du^k}{ds} = 0\,, \quad i = 1,2;$$

where Γ^i_{jk} are the Christoffel symbols (of the second kind):

$$\Gamma^i_{jk} = \frac{1}{2}\sum_l g^{jl}\left(\frac{\partial g_{ij}}{\partial u^k} + \frac{\partial g_{jk}}{\partial u^i} - \frac{\partial g_{ik}}{\partial u^j}\right);$$

and where:

$$g_{11} = E, g_{12} = g_{21} = F, g_{22} = G \text{ and } \left(g^{ij}\right) = \left(g_{ij}\right)^{-1};$$

is obviously not applicable in the case of PL surfaces. (It only serves to justify the following authoritative but, unfortunately usually forgotten fact ([7]): "There are extremely few surfaces on which geodesics (and a fortiori shortest routes) can be more or less explicitly determined.".

We can however try and apply the above condition $\kappa_g = 0$. Again, the differentiable formula for the computation of the geodesic curvature:

$$\kappa_g = \frac{1}{2\sqrt{EG}}\left[G_u\frac{dv}{dt} - E_v\frac{du}{dt}\right] + \frac{d\varphi}{dt}$$

is of little relevance for triangulated surfaces. Instead we can apply the following formula, due to Polthier and Schmies, and an extension of previous results of the Alexandrov school (see [1], [28]), for the computation of κ_g for curves on 2-dimensional polyhedral surfaces,

$$\kappa_g = \frac{2\pi}{\theta}\left(\frac{\theta}{2} - \beta\right).$$

More precisely, let γ be a PL curve γ on a polyhedral surface, and let $p \in \gamma$ be a vertex of the polyhedral surface. Then the *discrete geodesic curvature* of γ at p is given by following formula:

$$\kappa_g(\gamma, v) = \frac{2\pi}{\theta}\left(\frac{\theta}{2} - \beta\right)$$

where β represents a choice (i.e. the smallest) of the angle of γ at p – see Fig. 6 where δ represents the *discrete straightest geodesic* (at p), defined as in Fig. 7.

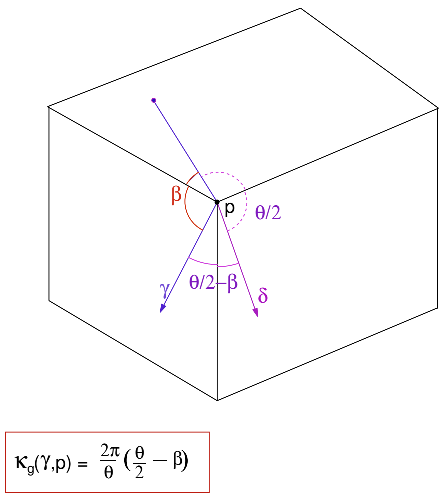

FIGURE 6. Discrete geodesic curvature at a vertex point of a polyhedral surface

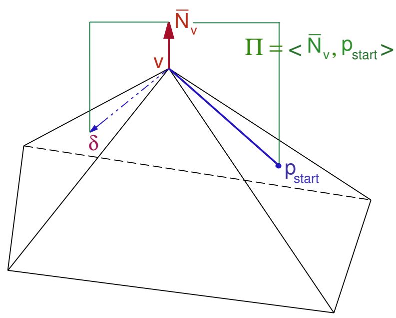

FIGURE 7. Straightest geodesic through a vertex point of a polyhedral surface

In this discrete approach to geodesic curvature, $\kappa_g(e) \equiv 0$, for any edge e. To include the geodesic curvature of the edges one can apply the the following formula:

$$\kappa_g(e) = \angle(\bar{N}_{v1}, \bar{N}_{v2})$$

where $\bar{N}_{v_1}, \bar{N}_{v_2}$ represent the *computed* normals at the vertices that define e (See. Fig. 8).

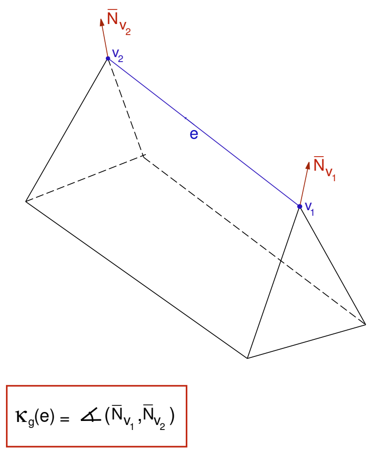

FIGURE 8. Discrete geodesic curvature along an edge of a polyhedral surface

3. Methods and Algorithms

3.1. Global Viewpoint. The algorithm that was used to find quasi-geodesic paths on the triangulated approximation of the colon surface is, essentially, we implemented the algorithm proposed in [27] (see also the discussion on PL-quasi-geodesics in Section 2.3 above), with the minor following additional constraint that that the path is allowed to run only along edges of the triangulation. Accordingly, for a given direction and a given initial vertex, the algorithm computes the straightest possible path which stretches from the given given vertex in the given direction, under the above limitation that it pathes along edges. Since we employed this method for determining "quasi-generators" on the very thin topological cylinders produced by the scanning process of the colon, the quasi-geodesics it produces are, in fact, proper geodesics (with the said proviso of running only on the edges of the triangulation).

3.2. Local Viewpoint – Gehring-Väisälä. We will present in this section the algorithm that is used for obtaining a quasi-isometric (flat) representation of a given surface. First assume the surface is equipped with some triangulation T. Let N_p stand for the normal vector to the surface at a point p on the surface.

Second, a triangle Δ, of the triangulation must be chosen. We will project a patch of the surface quasi-isometrically onto the plane included in Δ. This patch will be called the patch of Δ, and it will consists of at least one triangle, Δ itself. There are two possibilities to chose Δ, one is in a random manner and the other is based on curvature considerations. We will refer to both ways later. For the moment assume Δ was somehow chosen. After Δ is (trivially) projected onto itself we move to its neighbors. Suppose Δ' is a neighbor of Δ having edges e_1, e_2, e_3, where e_1 is the edge common to both Δ and Δ'.

We will call Δ' *Gehring compatible w.r.t* Δ, if the maximal angle between e_2 or e_3 and N_Δ (the normal vector to Δ), is greater then a predefined measure suited to the desired predefined maximal allowed dilatation and distortion, i.e. $\max\{\varphi_1, \varphi_2\} \geq \alpha$, where $\varphi_1 = \measuredangle(e_2, N_\Delta)$, $\varphi_2 = \measuredangle(e_3, N_\Delta)$; (cf. Equations (2.6), (2.7)).

We will project Δ' *orthogonally* onto the plane included in Δ and insert it to the patch of Δ, iff it is Gehring compatible with respect to Δ.

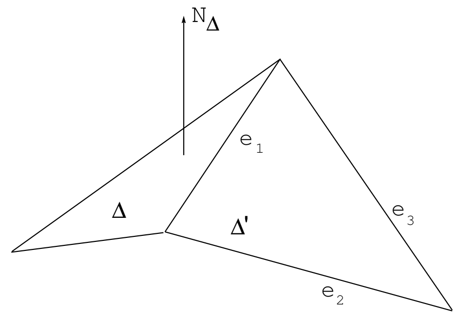

FIGURE 9. Gehring Compatible Triangles

We keep adding triangles to the patch of Δ moving from an added triangle to its neighbors (of course) while avoiding repetitions, till no triangles can be added. If by this time all triangles where added to the patch we have completed constructing the mapping. Otherwise, chose a new triangle that has not been projected yet, to be the starting triangle of a new patch. A pseudocode for this procedure can be easily written.

Remark 3.1. The algorithm was implemented in two versions, or more precisely two possible ways of processing, automatic versus user defined.

(1) Automatic means that the triangles serving as base points for the patches to be flattened are chosen automatically according to curvature, as stated in Remark 3.1. The discrete curvature measure employed is that of *angular defect*, due to its simplicity and high reliability (see [32]).
(2) User defined means that at each stage the user chooses a base triangle for some new patch.

Remark 3.2. One should keep in mind that the above given algorithm, as for any other flattening method, is local. Indeed, in a sense the (proposed) algorithm gives a measure of "globality" of this intrinsically local process.

Remark 3.3. Our algorithm is best suited for highly folded surfaces, because of its intrinsic locality, on the one hand, and computational simplicity, on the other. However, on "quasi-developable" surfaces (i.e. surfaces that are almost cylindrical or conical) the algorithm behaves similar to other algorithms, with practically identical results.

4. Experimental Results

4.1. **Quasi-geodesics and Conformal Modulus.** In this subsection we will present the results that where obtained when implementation of the algorithm for finding straightest quasi-geodesic path along the colon and the conformal modulus that was computed with respect to this presumably best cut of the colon surface in order to try and map it globally onto a flat region.

4.1.1. *Quasi-geodesics.* From every possible vertex on the top end of the surface (see figure below) the straightest path from it to the the bottom end was found. The figure shows the shortest of all thus obtained quasi-geodesics. This "quasi-shortest" path is the one by which the conformal modulus was assessed. Its length is 9.82.

4.1.2. *Conformal modulus.* Let γ be the shortest quasi-geodesic path found as above. Let its length be denoted by $L(\gamma)$ and as mentioned above equals 9.82. After cutting the colon surface along γ, the resulting surface is a topological rectangle denoted by Q. Yet, its top/bottom sides may be of different lengths (see figure below). Let $L_{max}\,(L_{min})$ denote the length of the longest (respectively shortest) length of these sides. In the context of Section 2.2.3 The quasi-geodesic path γ corresponds to the path γ of (2.11) while for the circle c we will shall employ L_{min}.

Using (2.10) and (2.11) we have that

$$\frac{L_{min}^2}{Area(Q)} = \frac{175.68^2}{2051} = 15.04 \leq M(Q) \leq 21.26 = \frac{2051}{9.82^2} = \frac{Area(Q)}{L_\gamma^2}$$

One can also make appeal to Formula (2.13) (or rather to its counterpart for quadrilaterals). For our purposes we shall compare the given irregular cylindrical surface C (i.e. colon slice) to the *mean cylinder* C_M, where the height and circumference of C_M are the mean height, 14, and circumference, 190, of C, respectively. By some elementary computations we find that the lower bound for $K = K_f$, in the case when $R \equiv C$ and $R' \equiv C_M$, is 1.5. While this appears to suggest that the mapping f is rather close to being conformal, recall that this is only a very crude estimate, based upon a rough averaging process. In fact, there are regions that can be mapped practically

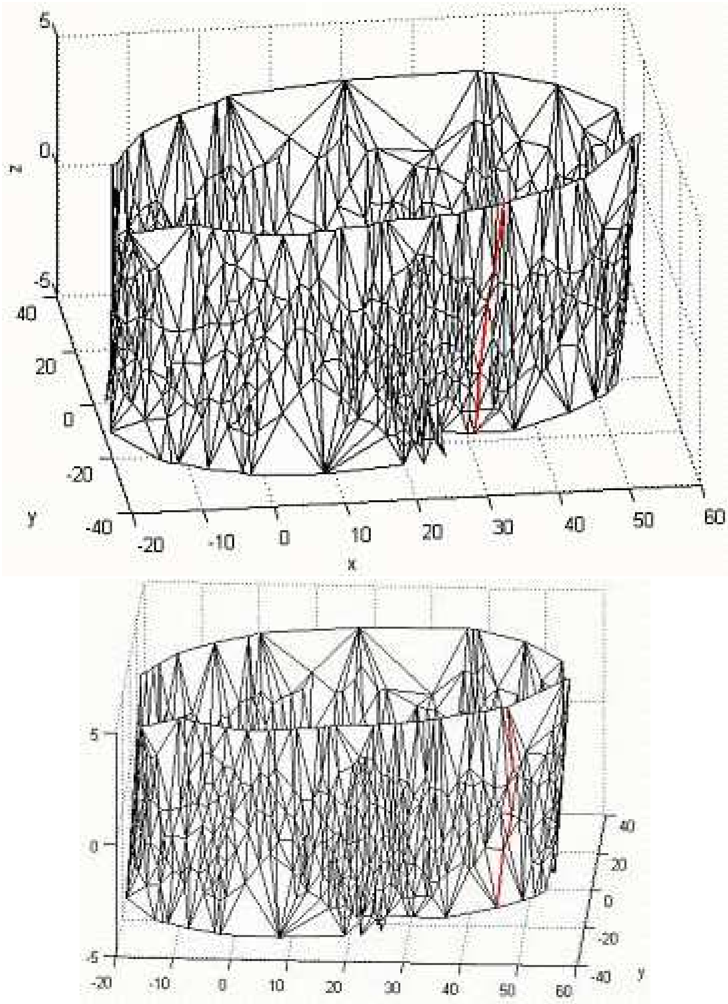

FIGURE 10. Two different views of the shortest quasi-geodesic on the "back side" of the colon surface.

conformally, and others where the required dilatation is extremely high (see Section 4.2 bellow and Figures 13, 14 and 15, therein).

4.2. **Flattening Algorithm.** We proceed to present and discuss experimental results obtained by applying the proposed algorithm for surface flattening, both on synthetic surfaces and on data obtained from CT scans. Different GUI's, each presenting specific fine tunings, were employed. A fully functional improved GUI, including all the features of the previous versions and a number of additional ones, allowing the implementation of all the described algorithms is currently under construction and will be available soon.

In each of the examples both the input surface and a flattened representation of some patch are shown. Details about mesh resolution as well as flattening distortion can also be provided, as well as the number of patches needed in order to flatten the whole surface.

The algorithm was implemented in two processing modes – automatic and user defined:

(a) Automatic means that the triangles serving as base points for the patches to be flattened are chosen automatically according to curvature (Section 3). The discrete curvature measure employed is that of *angular defect*, due to its simplicity and high reliability (see [33]).

(b) User defined means that at each stage the user chooses a base triangle for some new patch (e.g. Fig. 11 bottom).

Experiments have shown that results of the automatic process are similar, in terms of the dilatation, to those obtained from the user defined process yet, in order to flatten entire surface in the user defined method, one needs on the average 25% more patches. The need for gluing patches together into a global image is clear (and is well known in Radiography as the "*pantomograph*").

However, here we do not address the problem of properly gluing patches. Therefore, in the example depicting the flattening and gluing patches, of half of the triangulated surface obtained from 3 CT-scan slices of the human colon, there are "holes" in the flattened representation, caused by artificially gluing neighboring patches to each other (see Fig. 13).

Evidently, as made apparent by the colon flattening example above, one can have two neighbouring patches, with markedly different dilatations/distortions, which result in different lengths for the common boundary edges. Therefore, "cuts" and "holes" appear when applying a "naive" gluing. The discontinuities appear at the common boundary of two patches obtained from regions with very different curvature. Indeed, the "back part" (Fig. 14 top) seems close enough to be half of a cylinder (and thus *developable*) but in fact it is highly folded and creased (see Fig. 14 bottom).

In fact, the surface to be represented is a less flatter (topological) cylinder that visualized above, and with a "very bad" triangulation (Fig. 16, middle). This is a direct result of the scanning process, due to the difficulty to discern between colon and other tissues and between different folds of the colon (Fig. 16, bottom). This results in noisy data (Fig. 16, above) producing the "bad" triangulation observed.

Note that for small angles α (and hence for low dilatation/distortion) even non-simply connected patches may be obtained (e.g. Fig. 11 bottom, left). This is an immediate consequence of the algorithms' high sensitivity to curvature, quality that renders it highly suitable for discovering tumors, for instance in the colon, where they are associated with high curvature (Section 5).

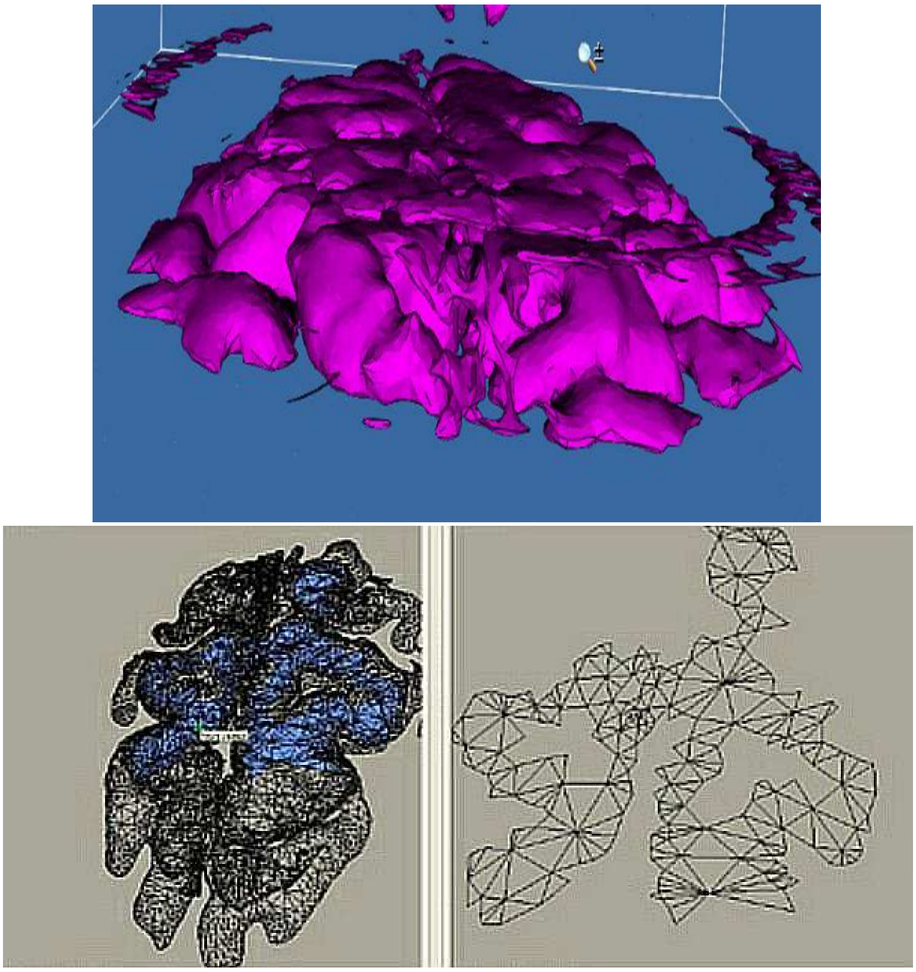

FIGURE 11. Flattening of 3D Cerebral Cortex data obtained by MRI. The resolution is $15,110$ triangles, the chosen angle of $5°$ produces a dilatations of 1.0875. The location of the cortical region selected for flattening (upper image) and a non-simply connected patch (bellow). Notice the position of the starting vertex for the flattening algorithm.

4.3. **(Black-and White) Images.** In recent years it became common amongst the image processing community, to consider images as Riemannian manifolds embedded in higher dimensional spaces (see, e.g. [18], [23], [29]), the embedding manifold usually being $\mathbb{R}^n$. For example, a gray scale image is a surface in $\mathbb{R}^3$, whereas a color image is a surface embedded in $\mathbb{R}^5$, each color channel representing a coordinate. In both cases the intensity, either gray scale or color, is considered as a function of the two spatial coordinates (x, y) and thus the surface may be equipped with a metric induced by this

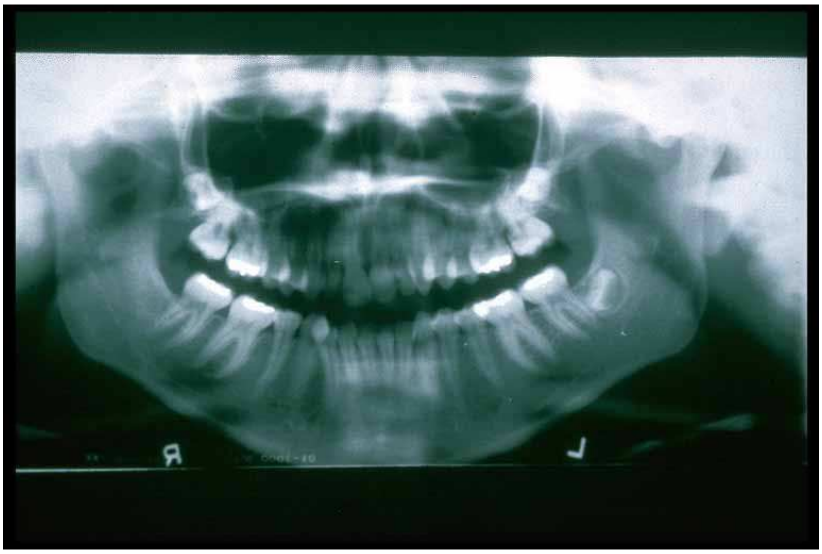

FIGURE 12. Pantomograph

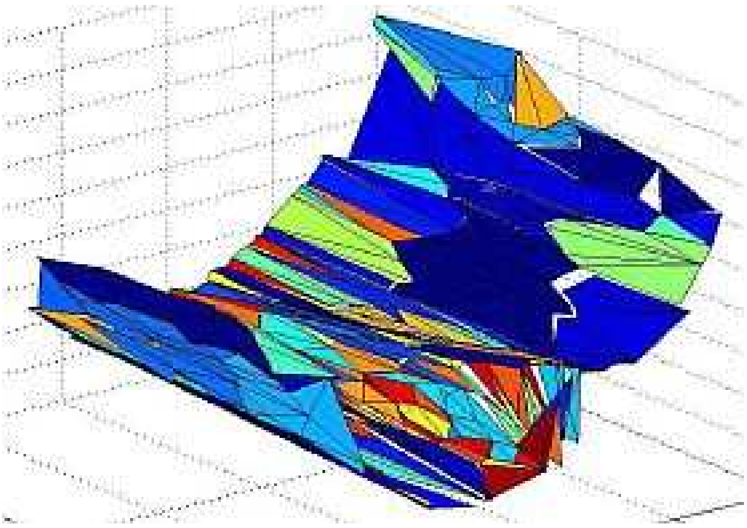

FIGURE 13. Colon Flattening: Image of one half of the triangulated colon surface taken from 3 slices. Note the "cuts" and "holes" due to a "naive" gluing method. Each color represents different flattened patch.

function. such a viewpoint of signals is the ability to apply mathematical tools traditionally used in the study of Riemannian manifolds, for image processing as well. For example, in medical imaging it is often convenient to treat CT/MRI scans, as Riemannian surfaces in $\mathbb{R}^3$. We bring bellow a

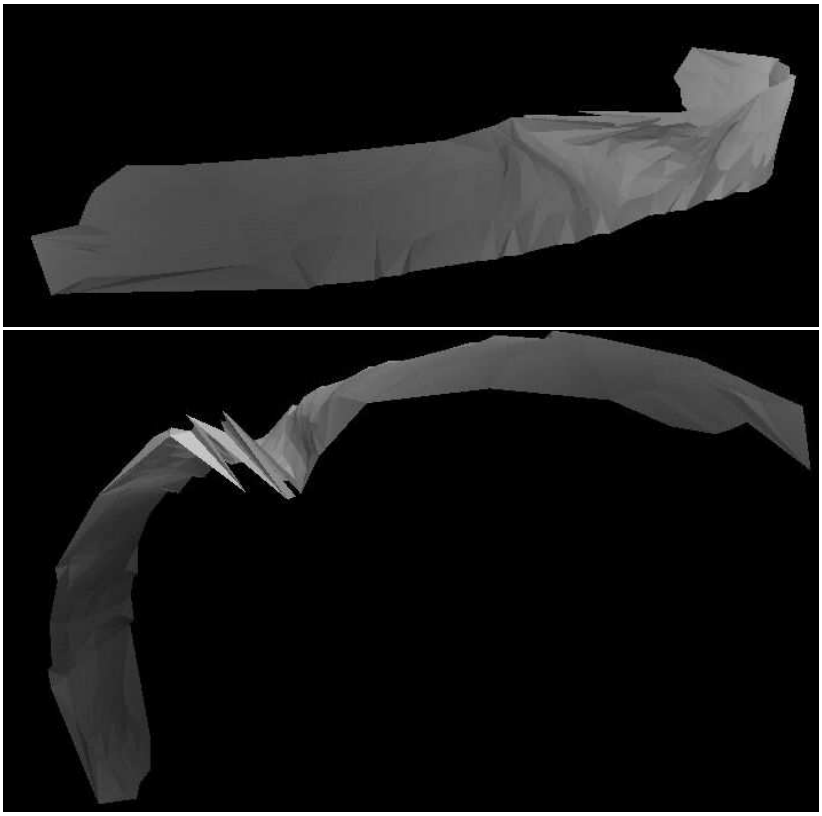

FIGURE 14. Colon CT-Images: Colon surface image taken from 3 slices of human colon scan. Images: curtesy of Dr. Doron Fisher from Rambam Madical Center in Haifa. Frontal view (upper image) and rotated image (bottom image) revealing the high degree of folding.

few remarks concerning the applications of quasiconformal mappings in this context.

Let D be a domain in $\mathbb{R}^{n-1}$ and let $u : D \to \mathbb{R}^1, u \in \mathcal{C}^1$ denote the grey scale (or luminosity) function. Define: $S = \{f(x) \,|\, x \in D\}$, where $f(x) = x + u(x)e_n$, $x \in D$, and where $e_n = (0, \ldots, 0) \in \mathbb{R}^n$.

Then

$$K_I(f) = K_O(f) = K(f) = \frac{1}{2^n}\left(a + \sqrt{a^2+4}\right)^n ;$$

where

$$a = \sup_{x \in D} |u'(x)| \,.$$

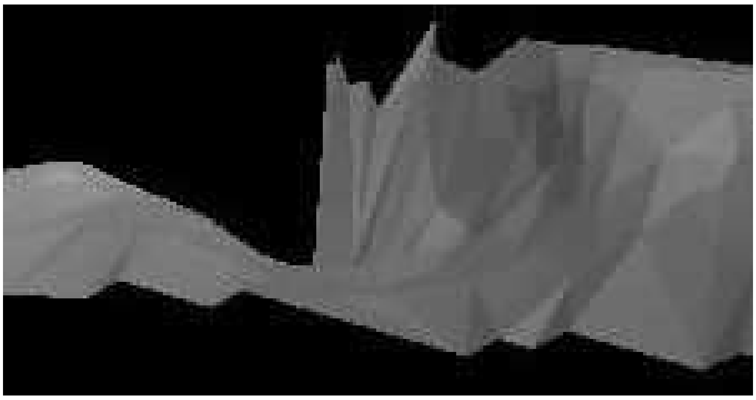

FIGURE 15. Colon CT-Images: Colon surface image taken from 3 slices of human colon scan. Another (detailed) view of the fold in the colon surface.

In particular, for the cases of practical interest in (medical) imaging, that is $n = 2, n = 3$ the maximal dilatation of f is $K(f) = \frac{1}{4}\left(a + \sqrt{a^2+4}\right)^2$, and $K(f) = \frac{1}{8}\left(a + \sqrt{a^2+4}\right)^3$, respectively.

Note that f is *qc* iff $a < \infty$. It also follows immediately that $K(f)$ is minimal for $a = 0$, that is for $u \equiv const$. This produces the expected – yet trivial – result that the dilatation of f, hence the that of the "photographic surface" is minimal for *gray shading*.

As already mentioned above, it is easier or more expedient in some cases to compute the linear dilatation (instead of the maximal dilatation). This holds for $n = 2$, for which we obtain:

$$H(x, f) \equiv \left(|u'(x)| - \sqrt{|u'(x)|^2 + 4}\right)^2$$

It is also possible to extend this method to include other features, such as RGB colours, luminosity, etc. in which case $D \subset \mathbb{R}^{n-k}$, where k stands for the number of added features $u_1, \ldots, u_k$, by defining $f(x) = x + \sum_{1 \leq i \leq k} u_i(x) e_{n-k+i}$.

We conclude this section by remarking that this application is perhaps less relevant for plane (2D) images, which, indeed, may be regarded only as a set of points of type $(x, y, u(x, y))$, where u is as above. Obviously the geometry of the domain of definition D is of no real relevance. To recapture a geometric content, one has, perhaps, to consider images as *drawings*, i.e. a set of relevant curves (to be considered, e.g. as ridges, ribs, level, curves, silhouettes, lines of curvature) on which an overlaying stratum of grey-scale/luminosity is added. However, note that $D = (S)$, and $f^{-1} = Pr$ thus $K(Pr) = K(f)$, where, as above, Pr denotes the orthogonal projection of S onto $\mathbb{R}^{n-1}$. Therefore, we thus obtain the maximal dilatation of the orthogonal projection of the gray-scale image onto the "hard-copy" photograph. Another possibility is to consider proper surfaces in $\mathbb{R}^3$, in which case the photographic surface is to be viewed (perhaps only locally) as a 4-dimensional hypersurface in $\mathbb{R}^5$.

5. Concluding Remarks and Future Study

From the implementation results it is evident that this simple to program as well as efficient algorithm, also yields good flattening results and maintains small dilatations even in areas where curvature is large and good flattening is a challenging task. Moreover, since there is a simple way to assess the resulting dilatation, the algorithm was implemented in such a way that the user can set in advance an upper bound on the resulting dilatation.

Contrary to some of the related studies, our algorithm does not require the use of derivatives. Consequently, the algorithm does not suffer from typical drawbacks of derivative-base computations. Moreover, since no derivatives are employed, no smoothness assumption about the surface to be flattened are made, which makes the algorithm presented herein ideal for use in cases where smoothness is questionable.

The algorithm may be practical use applications in cases where local yet good analysis is required, in medical imaging, emphasizing *accurate* and *measurable* flattened representation of the brain and the colon (virtual colonoscopy). We have noted in the previous section the algorithm's high sensitivity to curvature and the advantage this provides in the detection of carcinogen polyps in the colon. In this context, it is important to underline here the fact that quasi-conformal mappings, via the dilatation, are are highly sensitive to even *local* variations in the geometry of the surface under analysis. This renders them ideal to discern such minute variations, as produced by polyps and that may be smoothed out (by flow methods) or discarded as noise (by statistical methods). Another possible application would be in the mapping of the human brain, since high curvature regions are usually associated to more developed regions, and hence, for instance, to higher intelligence. (We are thankful to Prof. Koby Rubinstein who suggested this possible application). This type of application appears to be useful in Comparative Anatomy and Paleontology. Such directions of study are currently explored.

Further research is required however in processing from local to flat global image in a more precise fashion, i.e. how can one glue two neighbouring patches while keeping fixed bounded dilatation (i.e. to actually compute the *holonomy* of the surface – see [33].) Indeed, we may flatten the neighborhood of two vertices u, v, obtaining the flat images I_u, I_v, so that these two neighborhood have some intersection along the boundary yet, it will not be possible to adjust the resulting images to give one flat image $I_u \cup I_v$ of the union of these neighborhood which still keeping the quasi-isometric property. Here too, study is underway.

It should also be noted that, while the the application presented here is for $2D$-images of $3D$-surfaces, the results of Gehring and Väisälä are stated and proven for any dimension (and co-dimension). Therefore, implementations for higher dimensions are also understudy.

Indeed, since the importance of studying the elastic properties of images (i.e. that of isometries), as opposed to the rigid ones (i.e. quasi-isometries) has been already stressed in [24] (see also [35]), and since planar quasi-isometries almost preserve shape when strain is under the critical value ([11]), the application of quasi-isometries in higher-dimensional image processing and related fields is necessary. In particular, experimental results on the dilatation of grey-scale images (as considered in Section 4.3) are of significant practical interest and are also currently underway.

An additional promising direction of study stems from the theory of quasi-isometric/quasi-conformal mappings between admissible surfaces, with applications in face recognition.

Acknowledgment. Emil Saucan is supported by the Viterbi Postdoctoral Fellowship. Research is partly supported by the Ollendorf Minerva Center.

References

[1] Alexandrov, A. D. and Reshetnyak, Yu. G. *General Theory of Iregular Curves*, Mathematics and its Applications **29** , Kluwer, Dordrecht, 1989.

[2] Angenent, S., Haker, S., Tannenbaum, A. and Kikinis, R. *On Area Preserving Maps of Minimal Distortion*, System Theory: Modeling, Analysis, and Control, T. Djaferis and I. Schick, eds., pp. 275-287, Holland: Kluwer, 1999.

[3] Appleboim, E., Saucan E., and Zeevi, Y. *Minimal-Distortion Mappings of Surfaces for Medical Imaging*, Proceedings of VISAPP 2006.

[4] Appleboim, E., Saucan E., and Zeevi, Y. *Quasi-Conformal Flat Representation of Triangulated Surfaces for Computerized Tomography*, Lecture Notes in Computer Science **4241**, , Springer-Verlag, 2006.

[5] Appleboim, E., Saucan, E., and Zeevi, Y.Y. *On Sampling and Reconstruction of Surfaces*, Technion CCIT Report, 2006.

[6] Appleboim, E., Saucan E., Zeevi Y. Y.,and Zeitoun O., *Quasi-Isometric and Quasi-Conformal Development of Triangulated Surfaces for Computerized Tomography*, Lecture Notes in Computer Science **4040**, 361-374, Springer-Verlag, 2006.

[7] Berger, M. A Panoramic View of Riemannian Geometry, Springer-Verlag, Berlin, 2003.

[8] Cannon, J. W. *The theory of negatively curved spaces and groups*, Ergodic Theory, Symbolic Dynamics and Hyperbolic Spaces, Bedford, T., Kean, M. and Series, C.(Eds.), Oxford University Press, Oxford, 315-369, 1991.

[9] Caraman, P. *n-Dimensional Quasiconformal (QCf) Mappings*, Editura Academiei Române, Bucharest, Abacus Press, Tunbridge Wells Haessner Publishing, Inc., Newfoundland, New Jersey, 1974.

[10] do Carmo M. P.: Differential Geometry of Curves and Surfaces, Prentice-Hall, Englewood Cliffs, 1976.

[11] Gehring, W. F. *Topics in quasiconformal mappings* in Quasiconformal Space Mappings – A colection of surveys 1960-1990 (M. Vuorinen ed.), LNM **1508**, 20-38, Springer-Verlag, Berlin, 1991.

[12] Gehring, W. F. and Väisälä, J. *The coefficients of quasiconformality*, Acta Math. **114**, pp. 1-70, 1965.

[13] Gu, X. Wang, Y. and Yau, S. T. *Computing Conformal Invariants: Period Matrices*, Communications in Information and Systems, Vol. 2, No. 2, pp. 121-146, December 2003.

[14] Gu, X. and Yau, S. T. *Computing Conformal Structure of Surfaces*, Communications in Information and Systems, Vol. 2, No. 2, pp. 121-146, December 2002.

[15] Gu, X. and Yau, S. T. *Global Conformal Surface Parameterization* , Eurographics Symposium on Geometry Processing, 2003.

[16] Haker, S. Angenet, S. Tannenbaum, A. Kikinis, R. *Non Distorting Flattening Maps and the 3-D visualization of Colon CT Images*, IEEE Transauctions on Medical Imaging, Vol. 19, NO. 7, July 2000.

[17] Haker, S. Angenet, S. Tannenbaum, A. Kikinis, R. Sapiro, G. Halle, M. *Conformal Surface Parametrization for Texture Mapping*, IEEE Transauctions on Visualization and Computer Graphics, Vol. 6, NO. 2, June 2000.

[18] Hallinan, P. *A low-dimensional representation of human faces for arbitrary lighting conditions*, Proc. CVPR. pp. 995-999, 1994.

[19] Hilbert, D., Cohn-Vossen, S.: Geometry and the Imagination, Chelsea, 1952.

[20] Hsu, L., Kusner, R. and Sullivan, J. *Minimizing the Squared Mean Curvature Integral for Surfaces in Space Forms*, Experimental Mathematics, Vol. 1, No. 3, 191-201, 1992.

[21] Hurdal, M. K., Bowers, P. L., Stephenson, K., Sumners, D. W. L., Rehm, K., Schaper. K., Rottenberg, D. A. *Quasi Conformally Flat Mapping the Human Crebellum*, Medical Image Computing and Computer-Assisted Intervention -MICCAI'99, (C. Taylor and A. Colchester. eds), vol. 1679, Springer-Verlag, Berlin, 279-286, 1999.

[22] Hurdal, M. K. and Stephenson, K. *Cortical cartography using the discrete conformal approach of circle packings*, NeuroImage 23, 119-128, 2004.

[23] Kimmel, R. Malladi, R. and Sochen, N. *Images as Embedded Maps and Minimal Surfaces: Movies, Color, Texture, and Volumetric Medical Images*, International Journal of Computer Vision, **39**(2), pp. 111-129, 2000.

[24] Koenderink, J. J. *Solid Shape*, MIT Press, Cabmbridge, Mass., 1990.

[25] Lehto, O. and Virtanen, K. I. *Quasiconformal Mappings in the Plane*, Springer-Verlag, Berlin, 1973.

[26] Lev, R., Saucan. E. and Elber, G. *Curvature Estimation over Smooth Polygonal Meshes using The Half Tube Formula*, submitted, 2005.

[27] Polthier, K. and Schmies, M. *Straight Geodesics on Polyhedral Surfaces*, in Mathematical Visualization, Hege, H. C., Polthier, K., editors, Springer Verlag, 135-150, 1998.

[28] Pogorelov, A. V. *Quasigeodesic lines on a convex surface*, Amer. Math. Soc. Transl. I., ser. 6(72), 430-472, 1952.

[29] Seung, H. S. and Lee, D. D. *The Manifold Ways of Perception*, Science 290, 2323-2326, 2000.

[30] Stephenson, K. *personal communication.*

[31] Sheffer, A. de Stuler, E. *Parametrization of Faceted Surfaces for Meshing Using Angle Based Flattening*, Enginneering with Computers, vol. 17, pp. 326-337, 2001.

[32] Surazhsky, T., Magid, E., Soldea, O., Elber, G. and Rivlin E. *A Comparison of Gaussian and Mean Curvatures Estimation Methods on Triangular Meshes*, Proceedings of the IEEE International Conference on Robotics and Automation. Taipei, Taiwan, pp 1021-1026, September 2003.

[33] Thurston, W. *Three-Dimensional Geometry and Topology, vol.1, (Edited by S. Levy)*, Princeton University Press, Princeton, N.J. 1997.

[34] Väisalä, J. *Lectures on n-dimensional quasiconformal mappings*, Lecture Notes in Mathematics 229, Springer-Verlag, Berlin - Heidelberg - New-York, 1971.

[35] Wardetzky, M., Bergou, M., Harmon, D., Zorin, D., Grinspun, E. *Discrete Quadratic Curvature Energies*, to appear in Computer Aided Geometric Design, 2007.

Department of Electrical Engineering, Technion, Technion City, Haifa 32000

E-mail address: semil@ee.technion.ac.il
E-mail address: eliap@ee.technion.ac.il
E-mail address: ronen.lev@optitex.com
E-mail address: zeevi@ee.technion.ac.il

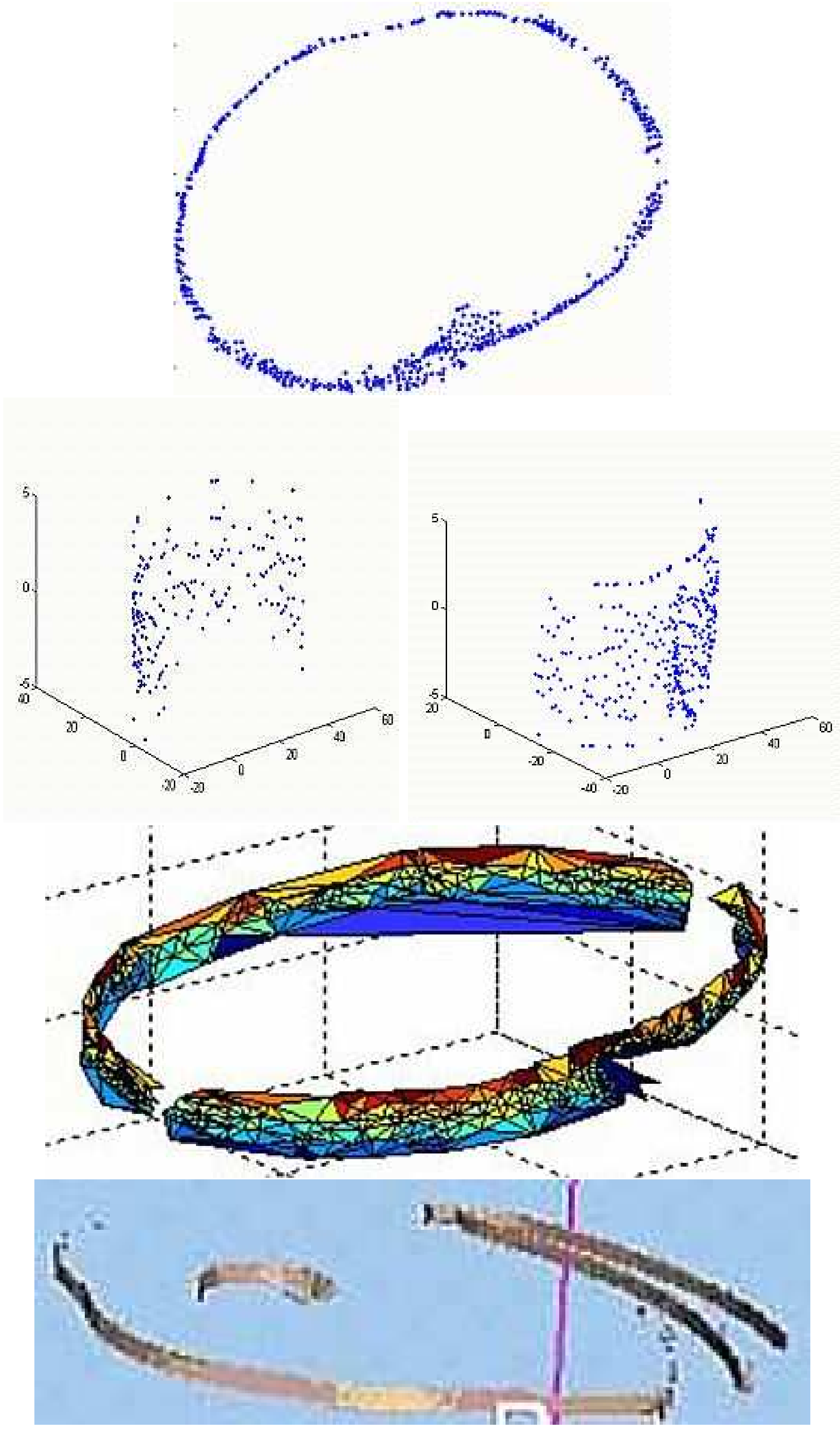

FIGURE 16. Colon CT-Images: noisy sampling (middle) producing an uneven triangulation (upper image) due to the difficulty in discerning the targeted tissue (bottom).

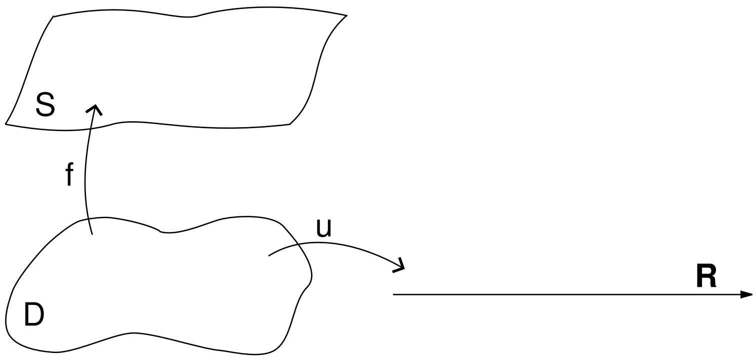

FIGURE 17. An abstract image as a surface given by the grey-scale hight function.